JOURNAL OF AIRCRAFT
Vol. 38, No. 4, July–August 2001

Flap-Deflection Optimization for Transonic Cruise Performance Improvement of Supersonic Transport Wing

Hyoung-Jin Kim,* Shigeru Obayashi,† and Kazuhiro Nakahashi‡
Tohoku University, Sendai 980-8579, Japan

Wing flap-deflection angles of a supersonic transport are optimized to improve transonic cruise performance. Toward this end, a numerical optimization method is adopted using a three-dimensional unstructured Euler code and a discrete adjoint code. Deflection angles of 10 flaps, five for leading edge and five for trailing edge, are employed as design variables. An elliptic equation method is adopted to enable interior grid modification during the design process. Interior grid sensitivities are neglected for efficiency. Also tested is the validity of the approximate gradient evaluation method for the present design problem; it is found to be applicable for leading-edge flap design in cases where there are no shock waves on the wing surface. The Broydon–Fletcher–Goldfarb–Shanno method is used to minimize the drag with constraints on the lift and upper surface Mach numbers. Two design problems are considered; one involves a leading-edge flap design, and the other involves simultaneous design of leading-edge and trailing-edge flaps. The latter gave a smaller drag than the former by about two counts. Successful design results suggest that the present design method is valid and efficient.

Introduction

BECAUSE of sonic boom restrictions, the next generation supersonic transport (SST) is required to cruise at a transonic speed over land, while cruising at a supersonic speed over water. To improve its transonic cruise performance, leading-edge (LE) and trailing-edge (TE) flaps have been considered as efficient tools that do not degrade supersonic cruise performance.[1,2] A SST wing cruising at a transonic speed is prone to flow separation because its leading edges are usually of much smaller nose radius or sharper than those of transonic transport wings. LE flaps can be very useful to avoid onset of flow separation in the transonic cruise regime.

Lovell[1] and Grenon[2] reported European research concerned with reducing drag at low speed and supersonic/transonic cruise conditions. In the references, LE flap optimization was adopted to improve transonic cruise performance and to avoid LE flow separation. Grenon[2] also reported the necessity of upward deflection of TE flaps in order to avoid flow separation near the wing tips.

In this study we employed five LE flaps and five TE flaps to improve transonic performance of an experimental supersonic transport, which is under development by National Aerospace Laboratory (NAL) of Japan. The flap-deflection angles are optimized using a gradient-based numerical optimization technique and a three-dimensional computational fluid dynamics (CFD) code.

With the advances in CFD and computing power of modern computers, aerodynamic design optimization methods utilizing CFD codes are more important than ever. Among several design optimization methods applicable to aerodynamic design problems, the gradient-based method has been used most widely because of its well-developed numerical algorithms and relatively small computational burden. In the application of gradient-based methods to practical aerodynamic design problems, one of the major concerns is the accurate and efficient calculation of sensitivity derivatives of an aerodynamic objective function. The finite difference approximation is the simplest way to calculate the sensitivity information because it does not require any sensitivity code. However, the accuracy of such an approach depends critically on the perturbation size of design variables and the flow initialization.[3] Recently, the complex variable method is drawing much attention as an accurate method for sensitivity calculation without any sensitivity analysis code because the method does not show dependency on the step size of design parameters.[4]

Sensitivity derivatives can be evaluated more robustly and efficiently by using a sensitivity analysis code based either on a direct method or an adjoint method. An adjoint method is preferable in aerodynamic designs because it is more economical when the number of design variables is larger than the total number of an objective function and constraints. Reuther et al.,[5] for example, designed aircraft configurations using a continuous adjoint method with Euler equations in a structured multiblock grid system.

For complex aerodynamic configurations the unstructured grid approach has several advantages over the structured grid approach. This approach allows treatment of complex geometry with greater efficiency and less effort. It also has a greater flexibility in the adaptive grid refinement/unrefinement; thus, the total number of grid points can be saved. Previous works on sensitivity analysis studies for unstructured grid approaches can be found in Refs. 5 and 6.

In this study we adopt a discrete adjoint sensitivity code developed by Kim et al.[6] from a three-dimensional unstructured Euler solver based on a cell-vertex finite volume method. Sensitivity derivatives of an objective function are calculated efficiently and accurately by the adjoint code. Flap-deflection angles are used as design variables. During the design process, interior grids are modified by the elliptic equation method. Grid sensitivities of the interior grids are neglected in order to reduce required computational time for the mesh sensitivity calculation.

The rest of this paper presents a brief review of the flow solver and the discrete adjoint code. Design methodologies are described including surface mesh deformation and interior mesh movement techniques. Design results utilizing the design method are finally given for the optimization of flap deflection angles of an SST wing. Design examples include LE flap-deflection optimization and a simultaneous optimization of LE and TE flaps.

Flow Analysis

The Euler equations for compressible inviscid flows are written in an integral form as follows:

Received 8 August 2000; revision received 18 January 2001; accepted for publication 19 January 2001.

*Postdoctoral Research Fellow, Department of Aeronautics and Space Engineering; currently Senior Researcher, Turbomachinery Research Department, Korea Aerospace Research Institute, Taejun 305-600, Republic of Korea. Member AIAA.

†Associate Professor, Department of Aeronautics and Space Engineering. Senior Member AIAA.

‡Professor, Department of Aeronautics and Space Engineering. Associate Fellow AIAA.

$$\frac{\partial}{\partial t}\int_{\P} \boldsymbol{Q}\,\mathrm{d}V + \int_{\partial f\P} \boldsymbol{F}(\boldsymbol{Q})\cdot\boldsymbol{n}\,\mathrm{d}S = 0 \tag{1}$$

where $\boldsymbol{Q} = [\rho,\ \rho u,\ \rho v,\ \rho w,\ e]^T$ is the vector of conservative variables; ρ the density; u, v, w the velocity components in the x, y, z directions; and e the total energy. The vector $\boldsymbol{F}(\boldsymbol{Q})$ represents the inviscid flux vector, and $\boldsymbol{n}$ is the outward normal of $\partial\Omega$, which is the boundary of the control volume Ω. This system of equations is closed by the perfect gas equation of state with a constant ratio of specific heats.

The equations are solved by an unstructured finite volume method using the cell-vertex scheme. For a control volume Eq. (1) can be written in an algebraic form as follows:

$$V_i\frac{\partial \boldsymbol{Q}_i}{\partial t} = -\sum_{j(i)} \Delta S_{ij}\boldsymbol{h}^{n+1}\left(\boldsymbol{Q}_{ij}^{+}, \boldsymbol{Q}_{ij}^{-}, \boldsymbol{n}_{ij}\right) \tag{2}$$

where ΔS_{ij} is a segment area of the control volume boundary associated with edge connecting points i and j. This segment area ΔS_{ij} as well as its unit normal $\boldsymbol{n}_{ij}$ can be computed by summing up the contribution from each tetrahedron sharing the edge. The term $\boldsymbol{h}$ is an inviscid numerical flux vector normal to the control volume boundary, and $\boldsymbol{Q}_{ij}^{+}$ are flow variables on both sides of the control volume boundary. The subscript of summation $j(i)$ means all node points connected to node i.

The numerical flux $\boldsymbol{h}$ is computed using an approximate Riemann solver of Harten–Lax–van Leer–Einfeldt–Wada.[7] The second-order spatial accuracy is realized by a linear reconstruction of the primitive gas dynamic variables $\boldsymbol{q} = [\rho, u, v, w, p]^T$ inside the control volume using the following equation:

$$\boldsymbol{q}(\boldsymbol{r}) = \boldsymbol{q}_i + \psi_i\nabla\boldsymbol{q}_i\cdot(\boldsymbol{r}-\boldsymbol{r}_i), \qquad (0\le\psi\le 1) \tag{3}$$

where $\boldsymbol{r}$ is a vector directed toward point (x, y, z) and i is the node index. The gradients associated with the control volume centroids are volume-averaged gradients computed by the surrounding grid cells. Venkatakrishnan's limiter[8] is used for the function ψ_i in Eq. (3) because of its superior convergence properties.

To integrate Eq. (2) in time, the lower-upper symmetric Gauss–Seidel(LU-SGS) implicit method[9] is adopted. With $\Delta\boldsymbol{Q} = \boldsymbol{Q}^{n+1} - \boldsymbol{Q}^{n}$ and a linearization of numerical flux term as $\boldsymbol{h}_{ij}^{n+1} = \boldsymbol{h}_{ij}^{n} + \boldsymbol{A}_i^{+}\Delta\boldsymbol{Q}_i + \boldsymbol{A}_j^{-}\Delta\boldsymbol{Q}_j$, Eq. (2) becomes the following equations:

$$\left(\frac{V_i}{\Delta t}\boldsymbol{I} + \sum_{j(i)}\Delta S_{ij}\boldsymbol{A}_j^{+}\right)\Delta\boldsymbol{Q}_i + \sum_{j(i)}\Delta S_{ij}\boldsymbol{A}_j^{-}\Delta\boldsymbol{Q}_j = \boldsymbol{R}_i \tag{4}$$

where $\boldsymbol{R}$ is a residual vector

$$\boldsymbol{R}_i = -\sum_{j(i)}\Delta S_{ij}\boldsymbol{h}_{ij}^{n} \tag{5}$$

The LU-SGS method on unstructured grid can be derived by splitting node points $j(i)$ into two groups, $j\in L(i)$ and $j\in U(i)$, for the second summation in the left-hand side of Eq. (4). The final form of the LU-SGS method for the unstructured grid becomes:

Forward sweep:

$$\Delta\boldsymbol{Q}_i^{*} = \boldsymbol{D}^{-1}\left[\boldsymbol{R}_i - \sum_{j\in L(i)}\Delta S_{ij}A_j^{-}\Delta\boldsymbol{Q}_j^{*}\right] \tag{6a}$$

Backward sweep:

$$\Delta\boldsymbol{Q}_i = \Delta\boldsymbol{Q}_i^{*} - \boldsymbol{D}^{-1}\sum_{j\in U(i)}\Delta S_{ij}A_j^{-}\Delta\boldsymbol{Q}_j \tag{6b}$$

where $\boldsymbol{D}$ is a diagonal matrix derived by Yoon and Jameson[9] with Jameson–Turkel approximation of Jacobian[10] as $\boldsymbol{A}^{\pm} = 0.5(\boldsymbol{A}\pm\rho_A\boldsymbol{I})$, where ρ_A is a spectral radius of Jacobian $\boldsymbol{A}$.

$$\boldsymbol{D} = \left(\frac{V_j}{\Delta t} + 0.5\sum_{j(i)}\Delta S_{ij}\rho_A\right)\boldsymbol{I} \tag{7}$$

The lower/upper splitting of Eq. (6) for the unstructured grid is realized by using a grid reordering technique[11] to vectorize the LU-SGS method and to improve the convergence.

Sensitivity Analysis

Direct Method

An aerodynamic sensitivity analysis begins with the fact that the discrete residual vector Eq. (5) of the nonlinear flow equations is null for a converged flowfield solution of steady problems. It can be written symbolically as

$$R_i[Q, \boldsymbol{X}, \beta] = 0 \tag{8}$$

where $\boldsymbol{X}$ is the grid position vector and β the vector of design variables. Equation (8) can be directly differentiated via the chain rule with respect to β to yield the following equation:

$$\frac{\mathrm{d}R_i}{\mathrm{d}\beta} = \left[\frac{\partial R_i}{\partial Q}\right]\left\{\frac{\mathrm{d}Q}{\mathrm{d}\beta}\right\} + \{C_i\} = 0 \tag{9}$$

where

$$\{C_i\} = \left[\frac{\partial R_i}{\partial X}\right]\left\{\frac{\mathrm{d}X}{\mathrm{d}\beta}\right\} + \left\{\frac{\partial R_i}{\partial\beta}\right\}$$

This equation is the direct sensitivity equation for the flow variable sensitivity $\{\mathrm{d}Q/\mathrm{d}\beta\}$. The vector $\{C_i\}$ has no relation with $\{\mathrm{d}Q/\mathrm{d}\beta\}$ and, thus, is constant throughout the solution process of the sensitivity equation for a design variable β. $\{\mathrm{d}X/\mathrm{d}\beta\}$ in the $\{C_i\}$ is a vector of grid sensitivity, which can be calculated by a finite difference approximation or the direct differentiation of a routine for the grid generation or modification.

To find the solution $\{\mathrm{d}Q/\mathrm{d}\beta\}$ of Eq. (9) iteratively, a pseudotime term is added as follows to obtain the incremental form:

$$V_i\frac{\partial \boldsymbol{Q}_i'}{\partial t} = \left[\frac{\partial R_i}{\partial Q}\right]\left\{\frac{\mathrm{d}Q}{\mathrm{d}\beta}\right\}^{(n+1)} + \{C_i\} \tag{10}$$

where $\boldsymbol{Q}'$ represents the solution vector $\{\mathrm{d}Q/\mathrm{d}\beta\}$. The preceding system of equations is solved with the LU-SGS scheme that is used for the flow solver. By comparing Eqs. (2) and (10), one notes that it is possible to obtain a direct sensitivity code by directly differentiating the right-hand side (RHS) of the flow solver.

When the flow variable sensitivity vector $\{\mathrm{d}Q/\mathrm{d}\beta\}$ is obtained, the total derivative of the objective function F can be calculated. The objective function F is usually an aerodynamic coefficient such as C_D, C_L, C_M, or a difference of surface pressures with a specified target pressure. The objective function F is a function of flow variables $\boldsymbol{Q}$, grid position $\boldsymbol{X}$, and design variables β, i.e.,

$$F = F[Q(\beta), X(\beta), \beta] \tag{11}$$

The sensitivity derivative of the cost function F with respect to a design variable β is given by

$$\left\{\frac{\mathrm{d}F}{\mathrm{d}\beta}\right\} = \left\{\frac{\partial F}{\partial Q}\right\}^{T}\left\{\frac{\mathrm{d}Q}{\mathrm{d}\beta}\right\} + \left\{\frac{\partial F}{\partial X}\right\}^{T}\left\{\frac{\mathrm{d}X}{\mathrm{d}\beta}\right\} + \left\{\frac{\partial F}{\partial\beta}\right\} \tag{12}$$

Adjoint Method

Because the total derivative of the flow equations in the steady state is null as can be seen in Eq. (9), we can introduce adjoint variables and combine Eqs. (9) and (11) to obtain

$$\left\{\frac{\mathrm{d}F}{\mathrm{d}\beta}\right\} = \left\{\frac{\partial F}{\partial Q}\right\}^T \left\{\frac{\mathrm{d}Q}{\mathrm{d}\beta}\right\} + \left\{\frac{\partial F}{\partial X}\right\}^T \left\{\frac{\mathrm{d}X}{\mathrm{d}\beta}\right\} + \left\{\frac{\partial F}{\partial \beta}\right\} + \{\lambda\}^T \left\{\left[\frac{\partial R}{\partial Q}\right]\left\{\frac{\mathrm{d}Q}{\mathrm{d}\beta}\right\} + \{C\}\right\} \tag{13}$$

Coefficients of the flow variable sensitivity vector $\{\mathrm{d}Q/\mathrm{d}\beta\}$ form the following adjoint equation:

$$\left[\frac{\partial R}{\partial Q}\right]^T \{\lambda\} + \left\{\frac{\partial F}{\partial Q}\right\} = 0 \tag{14}$$

If one finds the adjoint variable vector $\{\lambda\}$, which satisfies the preceding adjoint equation, one can obtain the sensitivity derivative of F with respect to β without any information about the flow variable sensitivity vector $\{\mathrm{d}Q/\mathrm{d}\beta\}$. This makes the computational cost for the sensitivity analysis independent of the number of design variables. Equation (13) eventually takes the following form:

$$\left\{\frac{\mathrm{d}F}{\mathrm{d}\beta}\right\} = \left\{\frac{\partial F}{\partial X}\right\}^T \left\{\frac{\mathrm{d}X}{\mathrm{d}\beta}\right\} + \left\{\frac{\partial F}{\partial \beta}\right\} + \{\lambda\}^T\{C\} \tag{15}$$

As with Eqs. (2) and (10), the adjoint equation (11) is also converted to the following system of linear algebraic equations with a pseudotime term added and is solved with the LU-SGS scheme:

$$\left[\frac{V_i}{\Delta t}\boldsymbol{I} + \sum_{j(i)} \Delta S_{ij} \boldsymbol{A}_i^{+^T}\right] \Delta\lambda_i - \sum_{j(i)} \Delta S_{ij} \boldsymbol{A}_i^{-^T} \Delta\lambda_j = R\_\mathrm{adj}_i \tag{16}$$

where R_adj_i is the adjoint residual defined as

$$R\_\mathrm{adj}_i = \left[\frac{\partial R}{\partial Q_i}\right]^T \{\lambda\} + \left\{\frac{\partial F}{\partial Q_i}\right\}$$

Flux Jacobian matrix A^- in the second summation is calculated at node i instead of node j and of negative sign. This shows that wave propagation direction of the adjoint equations is opposite to that of the flow equations. However, the information on grid reordering used in the LU-SGS routine of the flow solver for the convergence improvement and vectorization is still valid here for the adjoint equations.

All of the required differentiation for the sensitivity equations is conducted by hand differentiation. More details on the sensitivity analysis such as boundary conditions and code validation can be found in Ref. 6.

Design Methodology

Design Objective

The present design method using the unstructured Euler solver and the adjoint method is applied to an unpowered experimental SST, which is under development by NAL of Japan as a basic study for the next generation supersonic transport.[12]

The objective of the present design study is defined as follows:

Minimize C_D, subject to:

$$C_L = C_L^* \tag{17}$$

where C_D and C_L are drag and lift coefficients, respectively, and C_L^* is a specified target lift coefficient. If the lift constraint is dealt with as an explicit constraint in an optimizer, it requires an additional adjoint code computation for the C_L derivatives. In this study, therefore, the lift constraint is satisfied running the flow solver in a fixed-lift mode, in which the incidence angle α is adjusted based on $C_{L\alpha}$ to obtain a lift coefficient satisfying the following inequality conditions:

$$C_L^* \le C_L \le 1.003 C_L^* \tag{18}$$

Because we would like to minimize drag when $C_L = C_L^*$ at an adjusted incidence angle, the objective function $F = C_D$ should be modified as follows to consider the lift constraint consistently.[6]

$$F = C_D - \frac{(\partial C_D/\partial\alpha)}{(\partial C_L/\partial\alpha)}\left(C_L - C_L^*\right) \tag{19}$$

where C_L is a lift coefficient without any incidence angle variation. The second term on the RHS of Eq. (19) acts as a penalty term, which prevents the design from reducing the drag by simply reducing the lift. The same expression for the modified objective function was suggested in a variational form by Reuther et al.[5]

An additional constraint for the suppression of boundary-layer separation is required because the present design study is based on inviscid flow physics only. It is implemented by imposing upper bounds of effective Mach numbers on the wing surface as was employed in Refs. 1 and 2. The effective Mach number is calculated from actual local Mach number considering local sweep angle, which varies gradually from the LE sweep angle to TE sweep angle. The upper bound of the effective Mach number is 1.3 for the first half-chord and 1.1 for the second half-chord region. This constraint is treated as a penalty term added explicitly to the Eq. (19) as follows:

$$F_{\mathrm{new}} = F + w \sum_{\mathrm{surface}} \max(0,\, p_{\mathrm{lim}} - p_{\mathrm{surf}})\Delta S \tag{20}$$

where w is a weighting factor multiplied to the penalty term, p_{lim} is pressure limit calculated from the Mach number limit by the isentropic relation, and ΔS is an area of a surface grid cell.

Design Parameters and Grid Modification Method

In the present design study, design variables are deflection angles of 10 flaps: five LE and five TE flaps. Figure 1 shows definitions of LE and TE flaps on the main wing of the experimental SST. Chordwise length of all of the LE flaps is set to be 40% of the wing tip chord length, and TE flap length is defined to be 20% chord of TE kink location inboard and 20% chord of local sections outboard. Flap deflections are made such that each grid point on the flaps is translated along the z axis only according to its distance from the hinge line, and thus, wing planform is kept the same as the initial geometry. All flap angles are defined on a plane normal to the hinge line. Counterclockwise flap deflections are defined to be positive, i.e., downward deflections for LE flaps and upward deflections for TE flaps are positive.

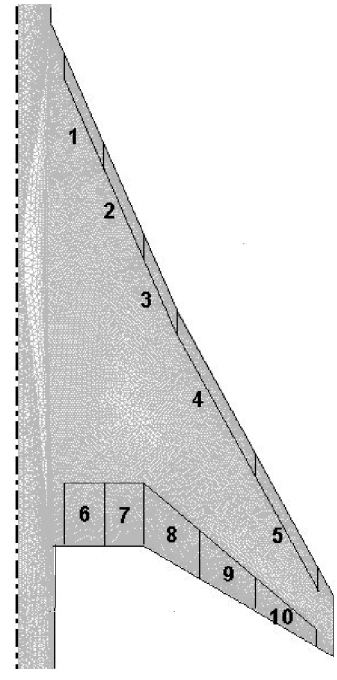

Fig. 1 Definition of LE and TE flaps.

Between every two flaps, wing surface geometry is linearly interpolated instead of being split. The thickness and camber of the wing section geometry is kept the same as the initial geometry so that supersonic cruise performance of the aircraft is not penalized by the flap design for transonic cruise.

When the surface grid is modified, the interior grid points should be moved accordingly. In the structured grid approach the interior grid positions can be moved with relative ease using an algebraic mesh movement strategy, which modifies the grid point coordinates along a grid line of the same index. In the unstructured grid method, however, such a simple grid modification method cannot be applied, and a more sophisticated grid movement method is needed.

For the movement of the grid points with the perturbed surface grid, we used the elliptic partial differential equation method proposed by Crumpton and Giles.[13] In the method the displacement δx from initial grid point x_0 is prescribed by the following equation with Dirichlet boundary conditions:

$$\nabla \cdot (k \nabla \delta x) = 0 \tag{21}$$

Diffusion coefficient k is constant in each cell and is given by

$$k = 1/\max(Vol, \varepsilon) \tag{22}$$

where Vol is a control volume of each grid point and ε is a small positive number to prevent k from becoming negative. The diffusion coefficient is inversely proportional to the cell volume so that a cell with a small volume goes under a rigid motion.

The elliptic equation (21) is discretized by a finite volume method, and subsequent linear algebraic equations are solved by the conjugate gradient method.[14] Required computational time to obtain converged solution δx was the same as that of a few iterations of the Euler solver.

Grid Sensitivity

The elliptic equation method for the interior grid movement is differentiated to be applied to the grid sensitivity calculation for the vector $\{C\}$ in Eq. (9) with respect to each geometric design variable. Because this requires almost the same computational cost as with the grid movement procedure, the total computational burden would be a substantial amount if the number of design variables becomes large.

One possible way to reduce the computational burden of the grid sensitivity calculation is to neglect the grid sensitivity of interior node points. It has been shown in Refs. 6 and 15 that in cases with inviscid flows interior grid sensitivity can be ignored for design variables not associated with a translation of a body. In this study, therefore, only the surface grid sensitivities are considered, and interior grid sensitivities for the flap deflection are ignored for efficiency.

Approximate Gradient Evaluation

Mohammadi[16] suggested the following approximate gradient evaluation, which neglects the sensitivity of an objective function with respect to flow variables when the objective function is based on a boundary integral:

$$\left\{\frac{\mathrm{d}F}{\mathrm{d}\beta}\right\} = \left\{\frac{\partial F}{\partial Q}\right\}^T \left\{\frac{\mathrm{d}Q}{\mathrm{d}\beta}\right\} + \left\{\frac{\partial F}{\partial X}\right\}^T \left\{\frac{\mathrm{d}X}{\mathrm{d}\beta}\right\} \cong \left\{\frac{\partial F}{\partial X}\right\}^T \left\{\frac{\mathrm{d}X}{\mathrm{d}\beta}\right\} \tag{23}$$

This approximation is based on an observation that the dominant part in the gradient is the partial derivative with respect to geometry and not to the flow variable when a small change in geometry causes very slight variations in flow variables. This would, of course, not be applicable to general cases, and, therefore should be adopted with great care. However, if it is found to be valid for a problem at hand, computational cost for the sensitivity analysis can be drastically reduced because any analysis of sensitivity equations is not required, and only the partial differentiation of the objective function with respect to geometry change is needed.

Optimization Method

For the unconstrained minimization of the objective function in Eq. (20), the Automated Design Synthesis program[17] was used as an optimizer. The Broydon–Fletcher–Goldfarb–Shanno method[18] is adopted in order to determine a search direction. One-dimensional search is then conducted using a quadratic polynomial interpolation. Detailed algorithms and methodologies of the optimization method are described in Ref. 18.

Design Results

Design conditions are a freestream Mach number of 0.95 and C_L of 0.2. Figure 2 shows the SST configuration and surface grids of initial geometry. The number of nodes and cells for the adopted volume grid are about 270,000 and 1,500,000, respectively.

Before we go on to the design optimization results, accuracy comparisons of sensitivity gradients are made for the simplification ignoring interior grid sensitivity and the approximate gradient evaluation using geometric sensitivity only. Figure 3 shows sensitivity derivatives of the objective function with respect to the 10 flap-deflection angles for initial geometry without any flap deflection. Derivatives obtained without interior grid sensitivity show good agreement with those calculated with surface grid sensitivity only. Similar results were also reported in a previous work by the authors[6] for supersonic flow conditions.

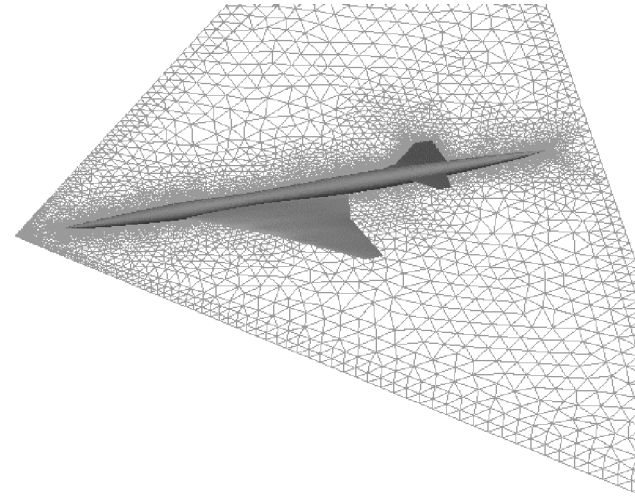

Fig. 2 Surface geometry of NAL experimental SST configuration and grids on symmetric plane.

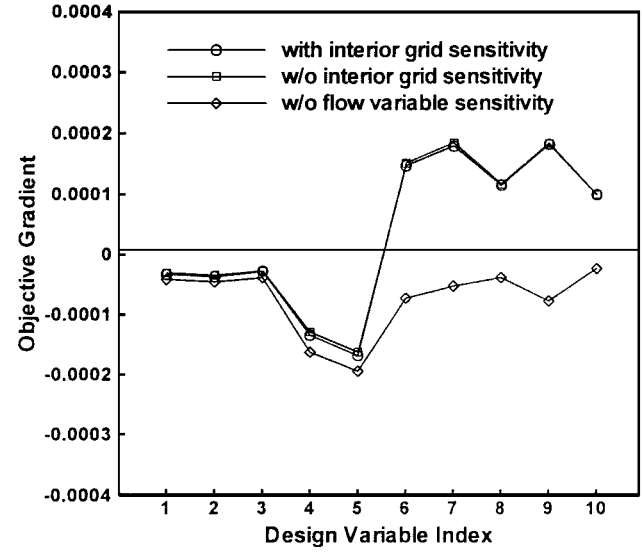

Fig. 3 Comparison of sensitivity derivatives for initial geometry.

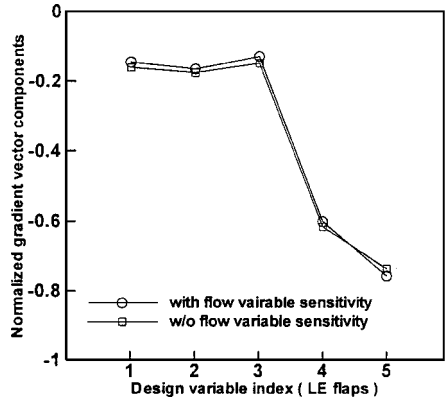

a) At initial geometry

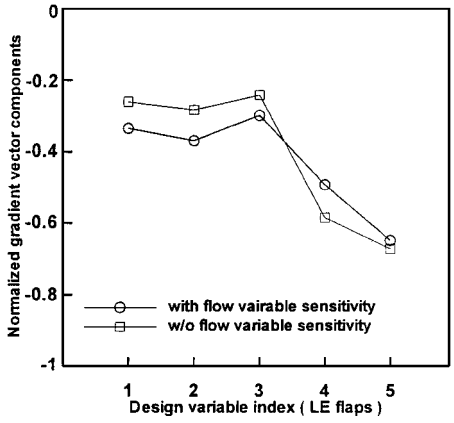

b) At design iteration two

Fig. 4 Comparison of normalized sensitivity derivatives.

In Fig. 3 sensitivity derivatives obtained by the approximate gradient evaluation method are also presented (diamond symbols). The derivatives with respect to the LE flap deflection calculated by the approximate gradient evaluation show similar trends to those obtained by the adjoint method, whereas those with respect to the TE flap have opposite signs with similar magnitude. This implies that deflection of LE flaps causes little change in flow variables, and therefore the effect of geometry change dominates in the total sensitivity derivatives for the present flow condition. On the other hand, for the TE flaps the variation of the flow variables caused by the flap deflection dominates in the total derivatives of the objective function. To compare the direction of the sensitivity derivative vector for LE flaps, normalized vector components are compared in Fig. 4a, which shows that the direction of the two vectors agrees well each other, although their magnitudes have some variations. This may allow us to get successful results of LE flap optimization with the sensitivity information obtained by the approximate gradient evaluation method.

In this study two design problems are considered: one involves an LE flap design, and the other involves simultaneous design of LE and TE flaps. We compared LE flap design results by the approximate gradient evaluation and by the adjoint method. For the LE and TE flap design the adjoint method is used because the approximate gradient evaluation does not give reliable sensitivity information for the TE flaps.

The density residual of the Euler solver was reduced by four orders from the initial value and that of the adjoint code by two orders. Lower and upper bounds of the 10 design variables are set as -30 and $+30$ deg, respectively, so that the design space is large enough and the design process is not disturbed by the bounds.

Design I: LE Flap Design

We conducted the LE flap design optimization by the approximate gradient evaluation and by the adjoint method with five flap-deflection angles as design variables. Although the approximate gradient evaluation gives accurate search direction for the initial geometry, the deviation of the normalized gradient vector components from the adjoint result increased to 15–30% as the design process continued to the second iteration as can be seen in Fig. 4b. This is because a shock wave was about to form on the upper surface, and the flow variable change as a result the LE flap deflection would increase drastically if a shock wave were to form on the wing surface.

Table 1 Results of design I; LE flap design

Compared items	Initial	Sensitivity derivative calculation method: Approximate gradient evaluation, (Δ, %)	Sensitivity derivative calculation method: Adjoint method, (Δ, %)
C_L	0.2002	0.2002 (0.0)	0.2000 (−0.1)
C_D	0.008087	0.006922 (−14.41)	0.006901 (−14.67)
L/D	24.76	28.93 (+16.84)	28.98 (+17.04)
Flap angle deg, (downward +)			
δ_1	0	4.63	6.18
δ_2	0	5.01	6.75
δ_3	0	4.40	5.76
δ_4	0	17.27	19.27
δ_5	0	17.10	19.99

Table 1 presents LE flap design results by the two sensitivity calculation methods. For both cases little improvement was achieved after the second design iteration, and the drag coefficient was reduced by about 12 counts retaining the lift coefficient as the specified value. Because of the increased inaccuracy of the approximate gradient evaluation, no perceivable flap-deflection changes were made after the first iteration, whereas the adjoint method provided accurate search direction so that flaps are deflected a few degrees more, and slight performance improvement was made accordingly. However, in spite of the inaccurate (but of right sign) sensitivity information of the approximate gradient evaluation after the second iteration, the difference of resulted drag coefficients was only about 0.2 count. This is because a local minimum solution was found by the first design iteration, and after that accuracy of the sensitivity derivatives seems not to affect the final results.

Comparing the results by the two methods shown in Table 1, one notes that LE flaps located inboard (flap #1, 2, and 3) show similar deflection angles, and the same is true for those located outboard (flap #4, 5). This implies that one may employ two flaps only; one for the inboard and the other for the outboard for a practical design of LE flap deflection for SST without major loss in aerodynamic performance.

Figure 5 shows surface pressure distributions at five wing sections that lie at the centerline of each LE flap. Leading-edge suction peaks have been reduced by the flap deflection, and the minimum pressure point occurs on the hinge line of the flaps. The surface Mach-number limits are not touched by the initial and design pressure distributions. The surface Mach-number limitation was the main factor that kept the LE flap angles from being increased more in Refs. 1 and 2. In the present example, however, it did not act as an active constraint, and thus, the penalty term in Eq. (20) was always zero during the design process. This is because of the fact that the SST wing adopted as an initial geometry of this study was designed using a natural laminar flow concept for the supersonic cruise condition, which made the LE of the wing very blunt.[12] The surface pressure contours on the wing's upper surface are depicted in Fig. 6. It is clear from this figure that the location of minimum pressure moved from LE to flap hinge line.

Design II: Design of LE and TE Flaps

In the present design example we tried to optimize the LE and TE flap angles with the design I obtained by using the approximate gradient evaluation method as the initial point. The sensitivity analysis showed that all of the TE flaps would be deflected downward to minimize the objective function. This is an interesting point reminding us of the necessity of upward deflection of TE flaps that was reported in Ref. 2 in order to avoid flow separation near the wing tips. We can expect that the direction and magnitude of TE flap deflection would be influenced by the performance improvement and by suppression of flow separation.

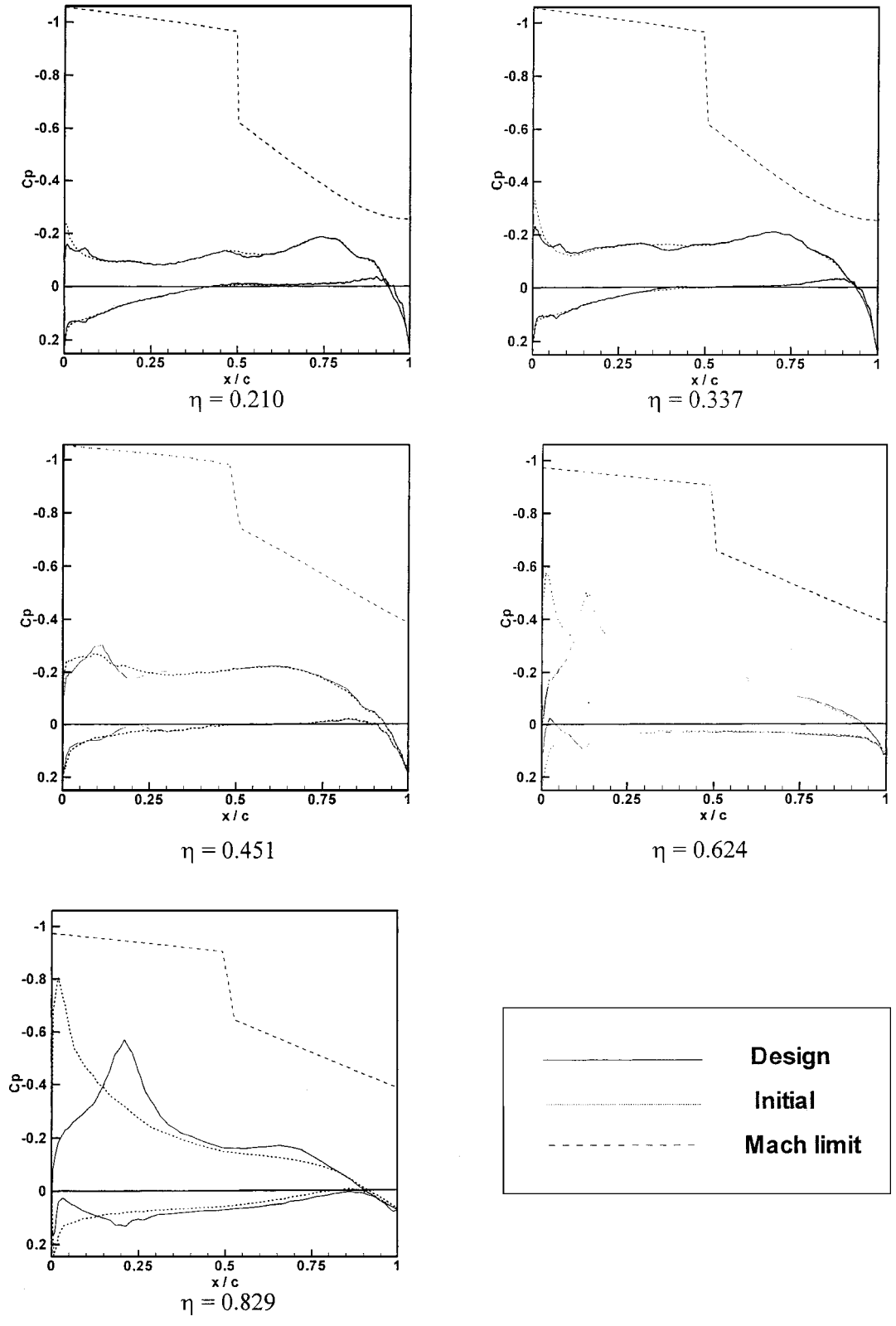

Fig. 5 Wing section surface pressure distributions (design I by AGE).

At the first optimization iteration it was found that the maximum Mach-number limit is a main factor that limits the deflection of inboard TE flaps, i.e., flap #6, 7, and 8. As a result, the downward deflection angles for the first iteration were only about 0.5 deg inboard and about 0.3 outboard, and the drag coefficient was reduced by about one-and-one-half counts. Figure 7 shows inboard section pressure distributions obtained by the one-dimensional search of the first iteration. Outboard pressure distributions do not differ much from those of design example I depicted in Fig. 5 and, therefore, are not presented here. The inboard flow is reaccelerated near the hinge of the TE flaps, and a shock appears just before the TE to recover the stagnation pressure. Although the solution did not violate the maximum Mach limit, it was still believed that it would promote flow separation in the real viscous flow as a result of the shock wave being too close to the TE. This was the case for a design with the

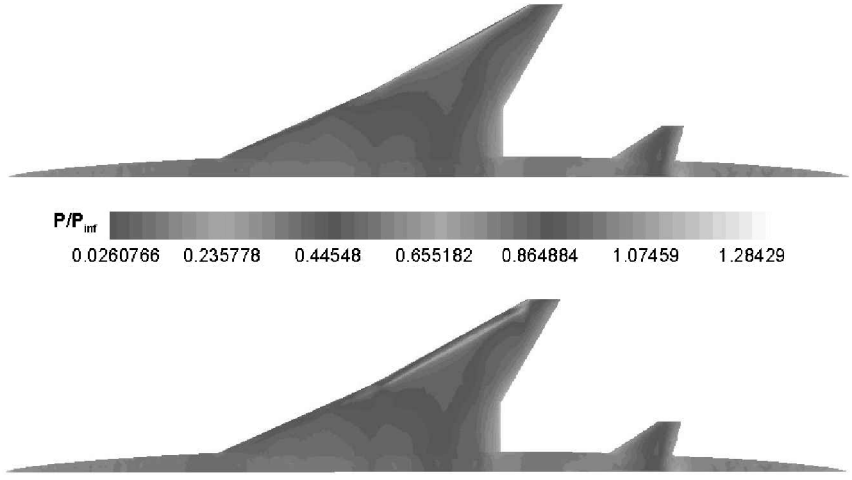

Fig. 6 Upper surface pressure contours of initial (up) and LE flap design (down) shapes.

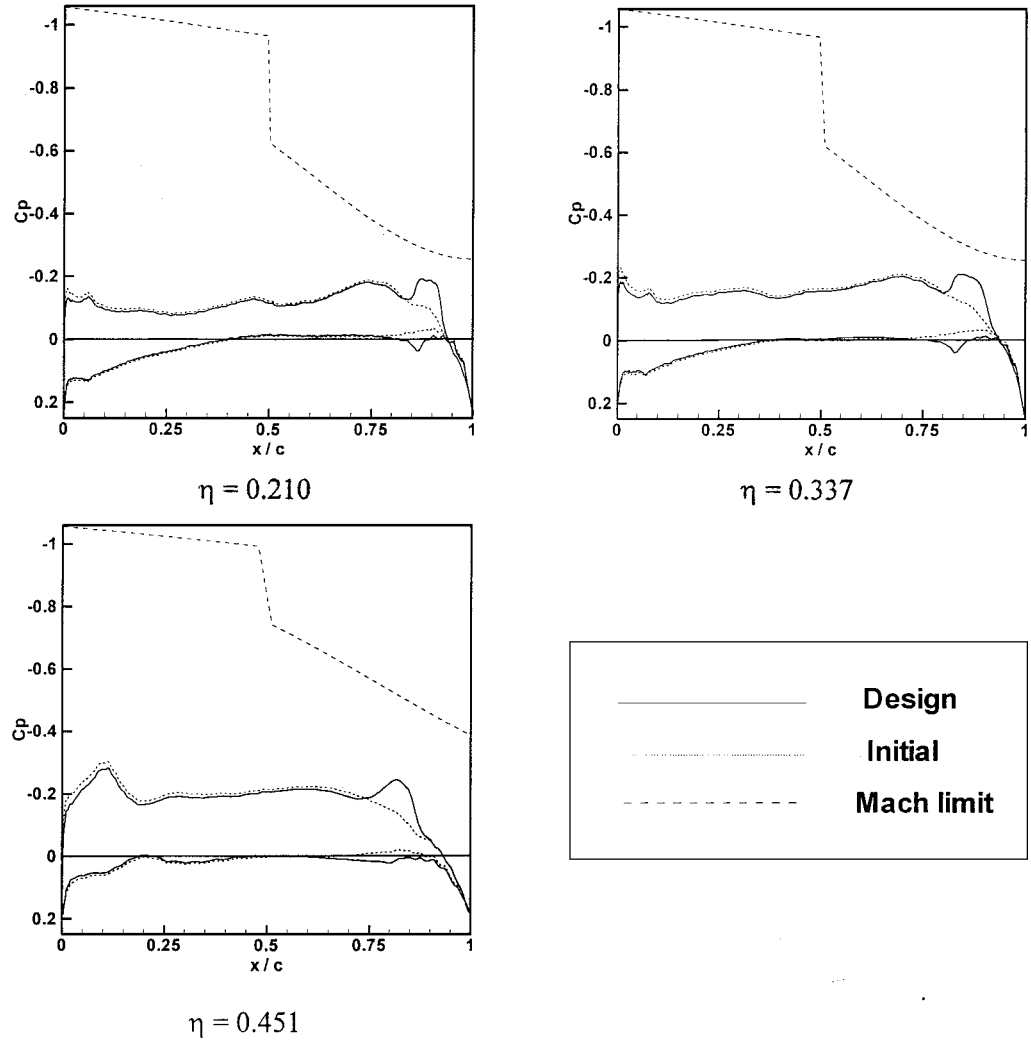

Fig. 7 LE and TE design results with inboard flap deflection activated; surface pressure distributions for inboard sections.

undeflected wing shape as an initial point. This shows the difficulty of imposing the maximum Mach-number limit on the wing surface. More sophisticated definition of Mach limits are required so that this kind of aerodynamic optimization problem can be attacked by using Euler codes rather than by more expensive Navier–Stokes computations.

Because the near-TE shock wave occurred for downward TE flap deflection of about 0.5 deg only, we decided to freeze (i.e., not to deflect) the inboard TE flaps (flaps #6, 7, and 8) and to design outboard flap deflections (flaps #9 and 10) only in addition to LE flaps. This design example was terminated after five iterations because there was no further performance improvement. Table 2 presents the LE and TE flap design results with inboard TE flaps frozen. Additional drag reduction of about two counts was made by the present design study from the optimized LE flaps of design I. Figure 8 shows surface pressure distributions of the design. Pressure

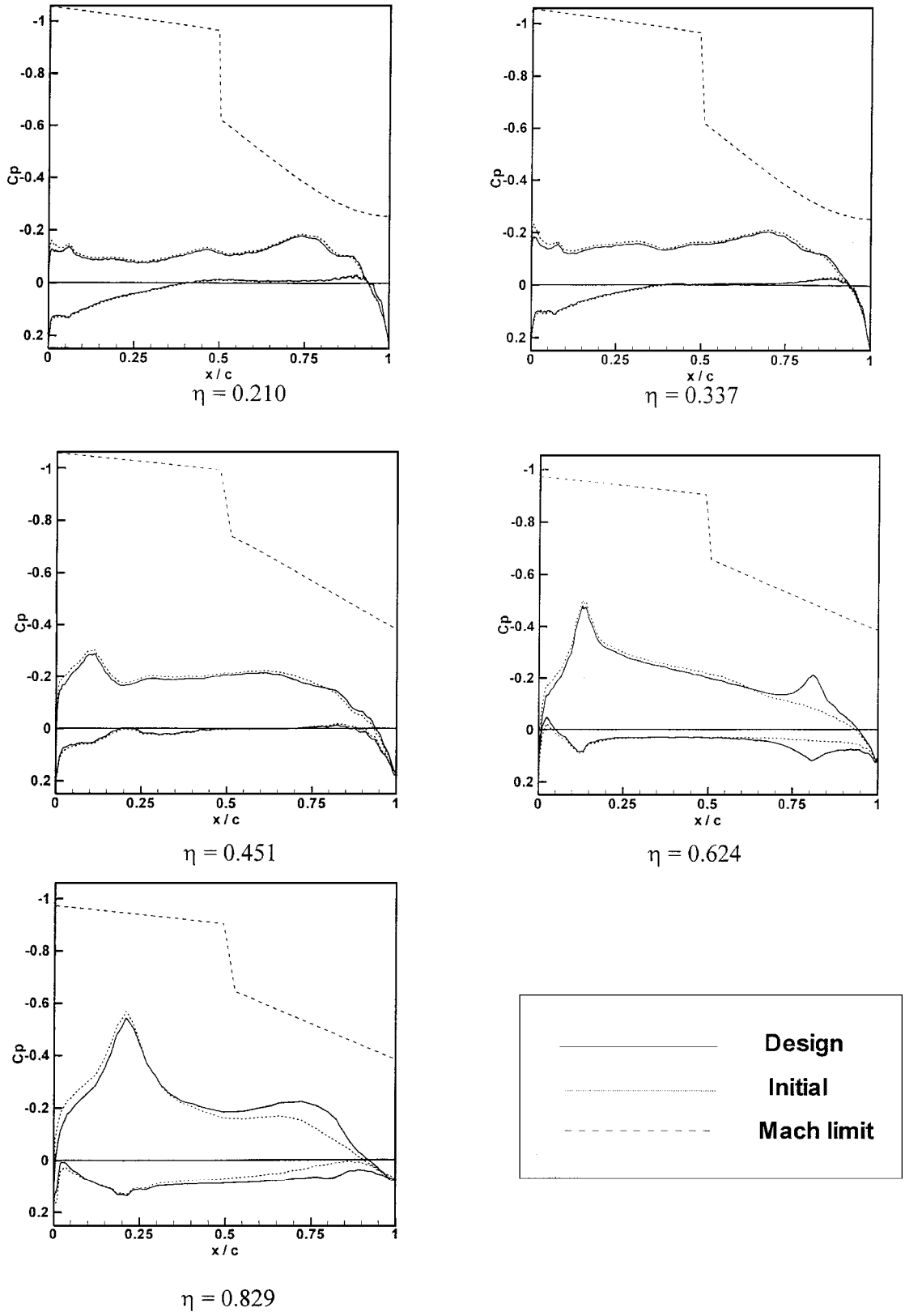

Fig. 8 LE and TE design results with inboard flap not activated; surface pressure distributions.

distributions of inboard sections show little difference from those of initial geometry except the fact that upper surface pressures have been slightly increased. This is because the downward deflection of TE flaps increased the lift, and therefore, the incidence angle was decreased to match the specified target lift coefficient. Outboard wing sections show the effects of TE flaps deflection; the flow is accelerated around the TE flap hinge line, and section lift is increased.

The outboard TE flaps can be deflected by about 2 deg without any shock waves, whereas the inboard LE flaps suffer from strong shock wave formation and flow separation with a deflection of merely 0.5 deg. This is because the TE sweep angle of the experimental SST of NAL is 30 deg outboard, while there is no TE sweep inboard. This sweep effect allows the outboard flow to have a higher separation margin than the inboard flow because the former has much lower effective Mach numbers on the wing surface near the TE than the latter.

Table 2 Results of design II; LE/TE flap design

Compared items	Initial	Design (Δ, %)
C_L	0.2002	0.1999 (−0.15)
C_D	0.006922	0.006723 (−2.88)
L/D	28.93	29.66 (+2.52)
Flap-deflection angles, deg		
LE (downward deflection +)		
δ_1	4.63	5.17
δ_2	5.01	5.60
δ_3	4.40	4.88
δ_4	17.27	18.00
δ_5	17.10	18.06
TE (upward deflection +)		
δ_6	0	0
δ_7	0	0
δ_8	0	0
δ_9	0	−2.26
δ_{10}	0	−1.68

Concluding Remarks

LE/TE flaps deflections are optimized to improve transonic cruise performance of a supersonic transport aircraft without degrading its supersonic performance. An aerodynamic design optimization system combining an optimization package, an unstructured Euler solver, and the discrete adjoint method was employed for efficient design studies. Deflection angles of five LE flaps and five TE flaps are defined as design variables. The approximate gradient evaluation method, which ignores the effect of flow variable change caused by the geometry perturbation on sensitivity derivatives, was found to be applicable to the design of LE flap angles; however, the approximate gradient evaluation method gives totally wrong sensitivity information for the TE deflections. By the design of LE flaps only, drag was reduced by about 12 counts, and the lift-over-drag ratio was increased by 17%. With this result as an initial point, a simultaneous design of LE/TE flaps was conducted to obtain additional two-count reduction of drag coefficient. Inboard TE flaps were frozen in order to avoid flow separation on the flaps. Deflection of outboard TE flaps had much less effect on flow separation than the inboard flaps because of the sweep back of outboard TE.

Acknowledgments

The first author was supported by the Japan Society for Promotion of Science. The authors also wish to thank Mr. Itoh, a graduate student of Tohoku University, for his help to generate the surface grid. The authors also thank to Dr. Iwamiya, National Aerospace Laboratory, for providing the surface geometry of National Aerospace Laboratory's experimental supersonic transport.

References

[1]Lovell, D. A., "European Research to Reduce Drag for Supersonic Transport Aircraft," AIAA Paper 99-3100, June 1999.

[2]Grenon, R., "Numerical Optimization in Aerodynamic Design with Application to a Supersonic Transport Aircraft," *Proceedings of the International Workshop on Supersonic Transport Design*, National Aerospace Lab., Tokyo, March 1998.

[3]Eyi, S., and Lee, K. D., "Effect of Sensitivity Calculation on Navier–Stokes Design Optimization," AIAA Paper 94-0060, Jan. 1994.

[4]Anderson, W. K., Whitfield, D. L., Newman, J. C., III, and Nielson, E. J., "Sensitivity Analysis for the Navier–Stokes Equations on Unstructured Meshes," AIAA Paper 99-3294, June 1999.

[5]Reuther, J. J., Jameson, A., Alonso, J. J., Rimlinger, M. J., and Saunders, D., "Constrained Multipoint Aerodynamic Shape Optimization Using an Adjoint Formulation and Parallel Computers, Part 1," *Journal of Aircraft*, Vol. 36, No. 1, 1999, pp. 51–60.

[6]Kim, H. J., Sasaki, D., Obayashi, S., and Nakahashi, K., "Aerodynamic Optimization of Supersonic Transport Wing Using Unstructured Adjoint Method," *AIAA Journal*, Vol. 39, No. 6, 2001, pp. 1011–1020.

[7]Obayashi, S., and Guruswamy, G. P., "Convergence Acceleration of an Aeroelastic Navier–Stokes Solver," *AIAA Journal*, Vol. 33, No. 6, 1995, pp. 1134–1141.

[8]Venkatakrishnan, V., "On the Accuracy of Limiters and Convergence to Steady State Solutions," AIAA Paper 93-0880, Jan. 1993.

[9]Yoon, S., and Jameson, A., "Lower-Upper Symmetric-Gauss-Seidal Method for the Euler and Navier–Stokes Equations," *AIAA Journal*, Vol. 26, No. 9, 1988, pp. 1025, 1026.

[10]Jameson, A., and Turkel, E., "Implicit Schemes and LU Decompositions," *Mathematics of Computation*, Vol. 37, No. 156, 1981, pp. 385–397.

[11]Sharov, D., and Nakahashi, K., "Reordering of Hybrid Unstructured Grids for Lower-Upper Symmetric Gauss-Seidel Computations," *AIAA Journal*, Vol. 36, No. 3, 1998, pp. 484–486.

[12]Iwamiya, T., "NAL SST Project and Aerodynamic Design of Experimental Aircraft," *Proceedings of the Computational Fluid Dynamics '98*, Vol. 2, ECCOMAS 98, Wiley, New York, 1998, pp. 580–585.

[13]Crumpton, P. I., and Giles, M. B., "Implicit Time Accurate Solutions on Unstructured Dynamic Grids," AIAA Paper 95-1671, June 1995.

[14]Press, W. H., Teukolsky, S. A., Vetterling, W. T., and Flannery, B. P., *Numerical Recipes in Fortran*, 2nd ed. Cambridge Univ. Press, Cambridge, England, UK, 1992, pp. 77–82.

[15]Anderon, W. K., and Venkatakrishnan, V., "Aerodynamic Design Optimization on Unstructured Grids with a Continuous Adjoint Formulation," AIAA Paper 97-0643, Jan. 1997.

[16]Mohammadi, B., "Flow Control and Shape Optimization in Aeroelastic Configurations," AIAA Paper 99-0182, Jan. 1999.

[17]Vanderplaats, G. N., "ADS—A Fortran Program for Automated Design Synthesis Version 3.00," Engineering Design Optimization, Inc., Santa Barbara, CA, 1987.

[18]Vanderplaats, G. N., *Numerical Optimization Techniques for Engineering Design: with Applications*, McGraw–Hill, New York, 1984, pp. 92, 93.